ORIGINAL ARTICLE

Application of the resistivity method in characterizing fractured aquifer in sedimentary rocks in Abakaliki area, southern Benue Trough, Nigeria

Ikenna A. Obasi[1] [ID] · **Nneka M. Onwa[2]** · **Ezekiel O. Igwe[3]**

Abstract

Resistivity range for groundwater-bearing fracture zones was studied in the fractured shales and sandstones of pre-Santonian sedimentary succession in Abakaliki area, southern Benue Trough, Nigeria using vertical electrical sounding (VES) data and borehole lithologs. The results of the study indicate that resistivity of water-bearing fracture zones in the shales is ≤ 52 Ωm and about 107 Ωm in sandstones. These fractures occur at a depth of ≥ 18 m in shales but shallower (≥ 6 m) in sandstones. The wider the fracture, the more the resistivity tends to zero, and the higher the volume of water present in it. While the layer models define the water-bearing layer, the synthetic model defines depth to the top of the fracture and fracture thickness. The wideness of the fractures decreases gradually below 80 m depth. The spatial distribution of resistivity in the area indicates that resistivity increases with depth except for the fracture zones.

Keywords Fractured shale · Aquifer · Benue Trough · Abakaliki · Groundwater

Introduction

Groundwater is one of the primary sources of freshwater globally and accounts for about one-third of the total supply of freshwater (Famiglietti 2014). Except for sand and gravel aquifers, groundwater is stored in hard-rock geological environments that are characterized by discontinuities such as fissures, voids, faults, and fractures (Demirel et al. 2018). Hard rocks, including crystalline igneous, metamorphic, and strongly cemented sedimentary and carbonate rocks, cover about 50% of the Earth's land surface (Singhal and Gupta 1999). Globally, the volume of groundwater contained in hard-rock aquifers is not well constrained (Comte et al. 2012), but locally they can be important aquifers (MacDonald et al. 2012).

Fractured sedimentary bedrock is an important source of water for many communities around the world (Steelman et al. 2017). The fracture zones within the rocks develop the hydrogeological characteristics which control groundwater occurrence and movement (Hasan et al. 2019). It can be best conceptualized as a dual-porosity system where fractures dominate flow, but remain connected to water stored in the porous matrix through advection and diffusion (Steelman et al. 2017). Locating subsurface fractures and their aquifer properties are key tools to successful groundwater exploration (Demirel et al. 2018; Chandra et al. 2019).

Common geophysical approaches associated with the study of weathered/fracture zones include the electrical resistivity, self-potential (SP), induced polarization (IP), borehole radar tomography, seismic reflection/refraction, ground-penetrating radar, and electromagnetic methods (Griffiths and Barker 1993; Improta et al. 2010; Carbonel et al. 2013). The resistivity method has always been applied in groundwater investigation (El-Hussaini et al. 1995; Vchery and Hobbs 2003; Tizro et al. 2010; Arabi et al. 2010), including hard-rock terrain (Barker et al. 1992; Carruthers and Smith 1992). Sometimes, it is integrated with fracture detecting geophysical techniques such as electromagnetic and seismic refraction methods (Adepelumi et al. 2006; Olorunfemi and Oni, 2019). Efforts at establishing the efficacy

✉ Ikenna A. Obasi
   obaik123@yahoo.com

1 Department of Geology, Federal University Lokoja, P.M. B. 1154, Kogi State, Nigeria

2 Department of Geology, University of Calabar, Calabar, Cross River State, Nigeria

3 Department of Geology, Ebonyi State University, P.M.B. 053, Abakaliki, Nigeria

of the electrical resistivity method in detecting such characters of fractures as density, aperture, and orientation in fractured rocks have been presented earlier in the literature using both field and laboratory approaches (Taylor and Fleming 1988; Jinsong et al. 2009; Berryman and Hoversten, 2013; Demirel et al. 2018). High-resistivity contrast is a major factor that differentiates fractured zones saturated with water from their fresh/unsaturated counterparts (Loke et al. 2003; Lucas et al. 2016; Hasan et al. 2018a). The resistivity method is sometimes integrated with borehole or well data in characterizing the subsurface for groundwater purposes (Hasan et al. 2019; Ammar and Kamal 2018). Drilled boreholes have been quite reliable in assessing subsurface information (Krasny 2002), although it could be quite tasking and costly (Akhter and Hasan 2016; Hasan et al. 2018a, b; Gao et al. 2018), especially in fractured rock aquifers (Ammar and Kamal 2018). Despite the large number of studies where resistivity methods have been applied to fractured rocks, qualitative and quantitative knowledge of how individual fractures influence resistivity data appears to be missing (Demirel et al. 2018). Consequently, the study of localized fracture systems in a given region is necessary to establish its peculiar response to current flow.

The Abakaliki area is predominantly underlain by Cretaceous shales of Asu River and Eze-Aku Groups with lenses of sandstones, mudstones, limestones (Okeke et al. 1987), and volcaniclastics (Chukwu and Obiora 2018), which have been tectonically deformed (Benkhelil 1989) to the extent that they got metamorphosed (Obiora and Charan 2011), and lost their primary porosities. The multiplicity of tectonism and magmatism, however, gave rise to faults, fractures, and weathered zones that are capable to act as aquifers. Urbanization and its associated problems of rural–urban migration, coupled with industrialization have enhanced population density in the area over time. Potable water supply by government agencies is quite inadequate (Aghamelu et al. 2013) to support the teeming population, and hence, the people resorted to self-help in the form of sinking private boreholes. An alternative supply of domestic water from ponds and other surface water sources in the area gave rise to an outbreak of dracunculiasis or dracontiasis otherwise known as Guinea worm disease (Anosike et al. 2003; Nnamani and Nnabueze 2012). Consequently, groundwater exists as the only safe source of potable water supply in the area. Location of these unevenly distributed water-bearing fracture systems has been a major barrier to potable water supply at economic quantity in the environment. Efforts of both government and non-governmental organizations (Wolfe 2007) at eradicating the guinea worm and remedy the situation through the provision of safe drinking water for the populace have been retarded due to series of abortive boreholes (Aghamelu et al. 2013). Poor knowledge of hydrostratigraphy, location of water recharge and discharge areas, and

their dynamic fluctuations with time (Akpan et al. 2013), as well as the subsurface distribution of fracture systems in the study area, have been identified as major causes of the abortive boreholes. None availability of other geophysical equipment known for their efficacy in fracture detection and low cost have favored the frequent use of the resistivity method in groundwater exploration in the study area. Much has not been done in characterizing the fractured aquifer systems in the area using the resistivity method. The resistivity values for water-bearing fracture zones in the shales are unknown. Their depth of occurrence is yet to be defined. Previous geophysical surveys for groundwater in the area (Ugwu and Nwosu 2009; Aghamelu et al. 2013; Odoh et al. 2012; Onwe et al. 2019; Agha 2015) have not been able to establish the resistivity values for the water-bearing zone in the area by integrating borehole and surface data. The aim of this work, therefore, is to characterize the groundwater-bearing fractures in the sedimentary rocks in Abakaliki area, southern Benue Trough Nigeria, by correlating geoelectric sections from vertical electrical sounding with borehole lithologs in the area.

Site description and geologic setting

The study area lies within Latitude $05^050'00''$ N–$06^040'00''$ N and Longitude $07^040'00''$ E–$08^030'00''$ E (Fig. 1). Murat (1970) identified three main tectonic phases in the trough which controlled the basin fillings. The first phase took place from Albian to Coniacian age. It was characterized by movements along major NE–SW-trending trough and led to the deposition of sediments of the Asu River Group (Albian), Eze-Aku Group (Turonian), and Awgu Formation (Coniacian), respectively. The Asu River Group consists dominantly of dark-gray shales which are baked in some places within the Abakaliki Anticlinorium, lenses of sandstones, and sandy limestones, volcaniclastics with subordinate mudstones (Benkhelil 1987). The Eze-Aku Group consists of thinly laminated, dark-gray flaggy shales with sandstones and subordinate limestones (Nwajide 2013; Petters 1980). It is conformably overlain by Awgu Formation in the western flank of Abakaliki Anticlinorium but abruptly missing in the eastern flank which is represented by Santonian angular unconformity in the region. The Awgu Formation consists of fissile, bluish-gray, pyritic, well-bedded shales with sandy or calcareous intercalations which are occasionally gypsiferous (Nwajide 2013). The second tectonic phase, which was a compressional movement, took place in the Santonian age. Widespread magmatism which accompanied the Santonian squeeze (Genik 1993) caused the southern Benue Trough to become flexurally inverted to form the Abakaliki Anticlinorium (Benkhelil 1987; Nwajide and Reijers 1996) and led to deposition of basic and intermediate intrusive igneous rocks
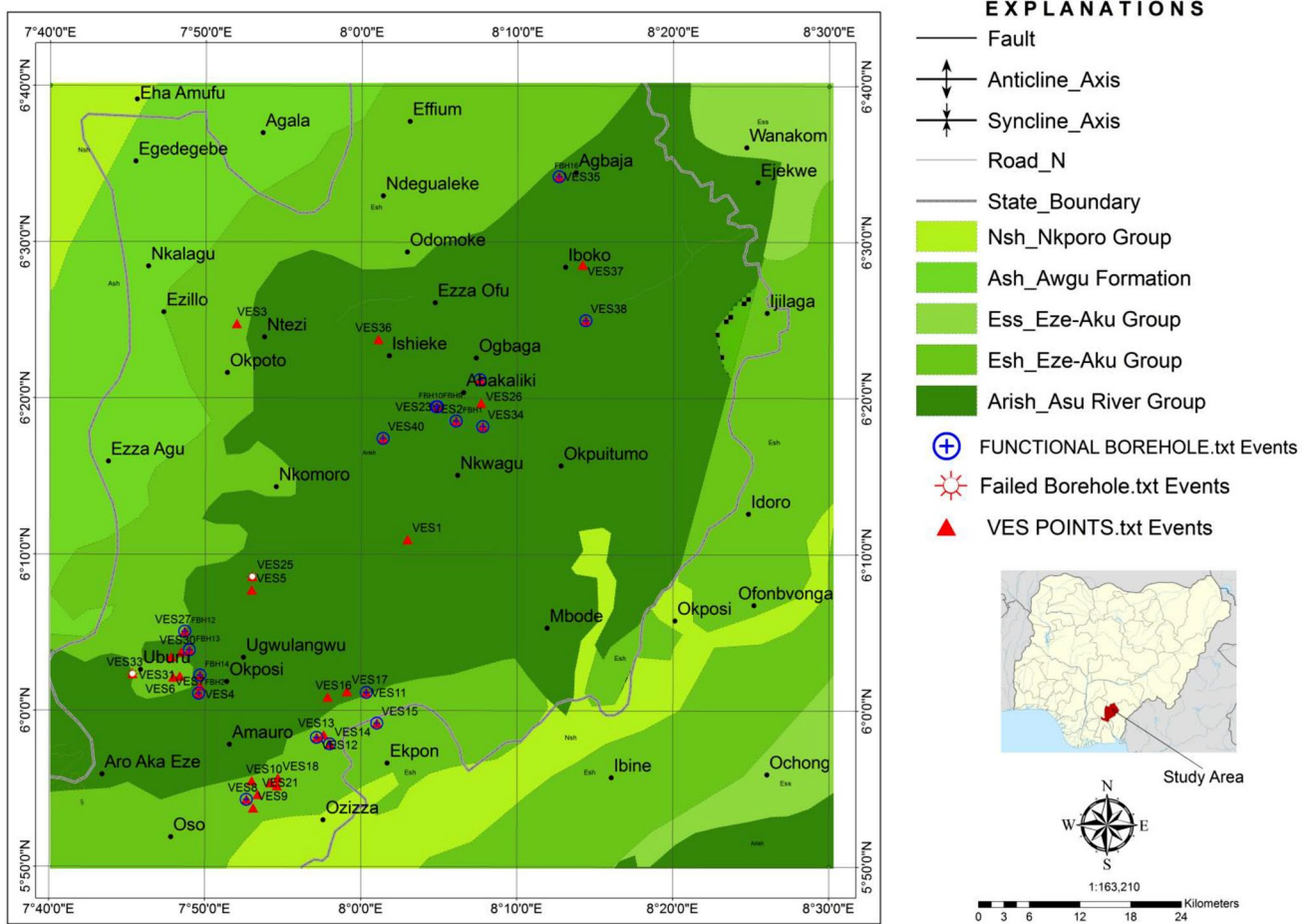
Fig. 1 Geologic map of the study area with VES and borehole points

in the shales in the area (Chukwu and Obiora 2014). Shales are naturally aquitards (Freeze and Cherry 1979); however, when they are tectonically and diagenetically altered, they develop some structural features like faults and fractures which serve as secondary porosity that is capable of hosting water at the economic quantity (Ebong et al. 2014; Macdonalds and Davies 1998). A combination of tectonism, magmatism during the Santonian Orogeny and post-depositional diagenetic alterations have highly deformed the rocks in the study area (Benkhelil 1987; Obiora and Charan 2011), baking the shales in some places (Okogbue and Nweke 2018) to a level of low-grade metamorphism (Obiora and Umeji 2004), while the sandstone members lost virtually all their primary porosities (Obasi and Selemo 2018), and gave rise to series of folds, faults, fractures, and fissures which host groundwater at economic quantity. In the absence of a primary aquiferous unit, the fractured units became major groundwater water supply units in the area.

The area has been previously identified as being hydrogeologically problematic (Offodile 1992). The Asu-River Group consists mainly of shales that are intensely fractured.

Except for fractured areas, the Asu River Group facies are extremely poor in groundwater prospects. Aquifers of the Eze-Aku Group are found in the sandstones and fractured limestones (Nwajide 2013).

Fig. 2 Field data acquisition using Schlumberger array at the Onueke Township Stadium

Table 1 Locations of the Vertical Electrical Sounding (VES) in the study area

VES No	Location	Latitude	Longitude
1	Onueke Township Stadium	$06^0 10' 57.9''$N	$08^0 02' 58.3''$E
2	Spera-in-Deo junction, Abakaliki	$06^0 18' 33.5''$N	$08^0 06' 05.3''$E
3	Evangel camp Okpoto	$06^0 24' 46.0''$N	$07^0 52' 00.0''$E
4	Onuogo Mebiowa, Okposi	$06^0 01' 34.2''$N	$07^0 49' 40.8''$E
5	Umuorie, Oshiri	$06^0 07' 43.0''$N	$07^0 52' 59.0''$E
6	Ogoachi, Okposi	$06^0 02' 07.9''$N	$07^0 47' 57.3''$E
7	Mebiowa, Okposi	$06^0 01' 06.6''$N	$07^0 49' 35.8''$E
8	Government Secondary School, Amasiri	$05^0 54' 18.9''$N	$07^0 52' 39.8''$E
9	Precious Foundation School, Amasiri	$05^0 53' 45.7''$N	$07^0 53' 05.5''$E
10	Ohia road, near Ejeke Primary School, Amasiri	$05^0 55' 29.8''$N	$07^0 52' 59.2''$E
11	Community Secondary School Abomege	$06^0 01' 10.7''$N	$08^0 00' 21.1''$E
12	Fishermen primary School Amata, Akpoha	$05^0 58' 17.3''$N	$07^0 57' 10.0''$E
13	Amata Primary School, Akpoha	$05^0 58' 27.0''$N	$07^0 57' 36.9''$E
14	Akpoha Central School	$05^0 58' 52.9''$N	$07^0 58' 00.3''$E
15	St. Benedict Primary School, Imina	$05^0 59' 12.4''$N	$08^0 01' 00.2''$E
16	Ohafia Ukawu, near Ukawu water scheme	$06^0 00' 52.2''$N	$07^0 57' 52.3''$E
17	Obina Central School, Ishinkwo Ukawu	$06^0 01' 13.6''$N	$07^0 59' 06.5''$E
18	Ibii junction, Ibii	$05^0 55' 40.3''$N	$07^0 54' 40.5''$E
19	Ibii - Amasiri road, Ibii	$05^0 55' 22.5''$N	$07^0 54' 13.3''$E
20	Ozaraukwu	$05^0 55' 11.2''$N	$07^0 54' 36.0''$E
21	Central School, Amasiri	$07^0 54' 37.5''$N	$07^0 53' 22.9''$E
22	Amike Aba, Abakaliki	$06^0 21' 12.0''$N	$08^0 06' 37.0''$E
23	PRESCO campus, Ebonyi State University	$06^0 19' 28.1''$N	$08^0 04' 48.6''$E
24	PRESCO campus, Ebonyi State university	$06^0 19' 27.7''$N	$08^0 04' 53.5''$E
25	Oshiri Health Centre, Oshiri	$06^0 08' 35.3''$N	$07^0 53' 01.3''$E
26	Azugwu, Abakaliki	$06^0 19' 42.0''$N	$08^0 07' 41.0''$E
27	Enuagu Community Primary School, Onicha	$06^0 05' 05.0''$N	$07^0 48' 42.0''$E
28	Ahia Nkwo market, Okposi	$06^0 03' 26.0''$N	$07^0 47' 50.0''$E
29	Isiama Health Centre, Onicha	$06^0 03' 53.0''$N	$07^0 49' 00.0''$E
30	Aja Nwachukwu Primary School, Okposi	$06^0 03' 49.0''$N	$07^0 48' 29.0''$E
31	Behind Federal Government College, Okposi	$06^0 02' 12.0''$N	$07^0 49' 23.0''$E
32	Holy Rosary Primary School, Okposi	$06^0 02' 16.0''$N	$07^0 49' 41.0''$E
33	Community High School Uburu	$06^0 02' 21.0''$N	$07^0 45' 21.0''$E
34	Inyimagu Azuiyiokwu, Abakaliki	$06^0 18' 12.0''$N	$08^0 07' 48.0''$E
35	Igwe kanyim, Oferekpe Agbaja, Izzi	$06^0 34' 13.0''$N	$08^0 12' 40.0''$E
36	Permanent site, Ebpnyi State University	$06^0 23' 46.0''$N	$08^0 01' 05.0''$E
37	Nwanu Community primary School, Izzi	$06^0 28' 33.2''$N	$08^0 14' 11.0''$E
38	Boys Secondary school, Iboko	$06^0 24' 59.6''$N	$08^0 14' 23.7''$E
39	Presco campus, Ebonyi State University	$06^0 19' 27.0''$N	$08^0 04' 52.0''$E
40	Umuoghara, Ezza North	$06^0 17' 26.0''$N	$08^0 01' 24.0''$E

Materials and methods

Equipment used for the geophysical survey includes a Global positioning system (GPS), Abem Terrameter SAS 1000, four electrodes, and four reels of Cables, a Direct Current Source, Survey Datasheets, and measuring tapes. The field layout is as shown in Fig. 2. Geoelectrical resistivity measurements were performed using the popular Schlumberger electrode configuration at forty (40) locations within the study area (Table 1), with the half current electrode separation $(^{AB}/_2)$ starting from 1 m up to 100 m in successive steps and 0.25 m to 10 m spacing for the potential electrodes. According to Lowrie (2007), using four electrodes comprising a pair of current electrodes labeled A and B, and a pair of potential electrodes labeled C and D respectively, the potential at electrode C is as given in Eq. (1). The potential at electrode D is represented in Eq. (2). The overall potential measured by the voltmeter connected between the potential

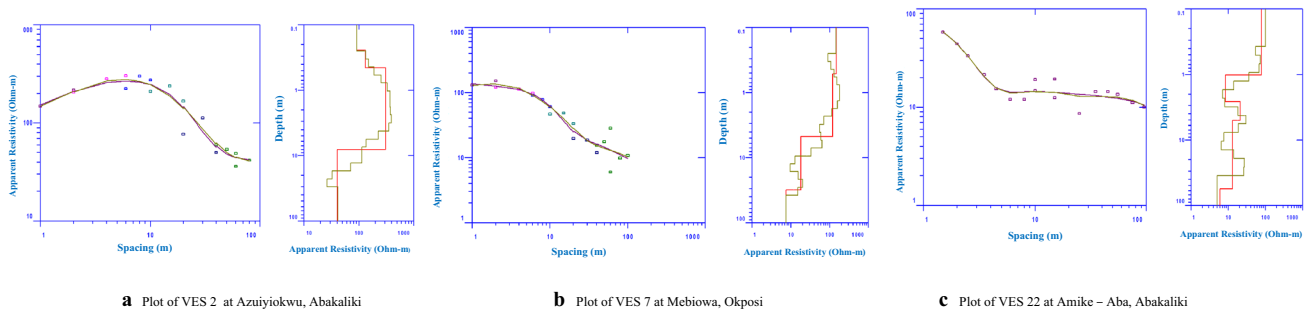**Table 2** Results of VES survey in the study area

VES No	Resistivity (Ωm)	Thickness (m)	Depth (m)	Inferred Lithology	Curve Type
1	289.36	0.5	0.5	Top soil	K
	297.88	6.99	7.5	Shale	
	50.41	104.14	111.63	Fractured shale	
	5475.6			Sandstone	
2	91.12	0.24	0.24	Top soil	K
	131.97	0.21	0.45	shale	
	309.74	7.62	8.07	shale	
	40.32			Fractures shale	
3	6253.5	0.35	0.35	Sandstone	HK
	128.13	0.64	0.99	Shale	
	3767.2	3.71	4.7	Sandstone	
	12.55	10.07	14.78	Fractured shale	
	956.89			sandstone	
4	64.56	0.64	0.64	Top soil	HK
	68.6	13.11	13.76	shale	
	29.85	29.07	42.82	Fractured shale	
	230.36			shale	
5	239.41	1.44	1.44	Top soil	HK
	78.37	5.3	6.74	shale	
	7388.2	0.21	6.96	sandstone	
	23.39	10.23	17.19	Fractured shale	
	4645			sandstone	
6	268.37	0.32	0.32	Top soil	HQ
	67.24	10.59	10.91	Shale	
	12.07	11.37	22.27	Fractured shale	
	146.42			shale	
7	148.67	0.51	0.51	Top soil	Q
	119.64	4.17	4.68	shale	
	18.12	26.69	31.37	Fractured shale	
	7.38			Fractured shale	
8	101.84	2.31	2.31	Top soil	H
	0.21	0.11	2.42	clay	
	385.08			shale	
9	0.33	0.74	0.74	Top soil	HK
	67			Shale	
10	73.28	0.85	0.85	Top soil	HQ
	40.69	7.27	8.12	shale	
	0.35	0.92	8.22	clay	
	50.15	57.35	65.56	Fractured shale	
	11.86			Fractured shale	
11	81.46	0.79	0.79	Top soil	H
	24.63	30.75	31.55	Fractured shale	
	327.9			Shale	
12	228.15	2.22	2.22	Top soil	Q
	95.53	23.75	25.97	shale	
	32.73	34.74	60.71	Fractured shale	
	2245.8			Sandstone	
13	250.11	2.2	2.2	Top soil	Q
	36.5	169.22	171.42	Fractured shale	
	10.74			Fractured shale	

Table 2 (continued)

VES No	Resistivity (Ωm)	Thickness (m)	Depth (m)	Inferred Lithology	Curve Type
14	396.39	1.6	1.6	Top soil	HQ
	10.44	0.43	1.64	Clay	
	570.47	3.26	4.9	Shale	
	179.37	20.68	25.59	shale	
	14.46	2.94	28.53	Fractured shale	
	1142			Sandstone	
15	29,156	0.32	0.32	Sandstone	HQ
	594.17	5.59	5.92	Sandstone	
	917.73	12.27	18.18	Sandstone	
	4.38	1.21	19.4	Fractured shale	
	549.69			Shale	
16	343.66	1.69	1.69	Top soil	Q
	372.09	7.77	9.46	Shale	
	97.48	127.28	136.74	Shale	
	1.76			Fractured shale	
17	1420.4	0.59	0.59	Top soil	H
	2192.5	1.12	1.72	Sandstone	
	1.98	0.18	1.73	clay	
	34.61	4.38	6.11	S hale	
	2050.7			Sandstone	
18	140.58	0.78	0.78	Top soil	HK
	4734.7	0.37	1.15	Sandstone	
	128.07			Shale	
19	192.65	1.95	1.95	Top soil	H
	2.22	0.28	2.23	clay	
	258.55			shale	
20	182.6	2.12	2.12	Top soil	HQ
	6.79	3.28	5.4	clay	
	15,743	136.05	141.45	Sandstone	
	4.27			Fractured shale	
21	44.59			shale	K
22	78.14	1.01	1.01	Top soil	Q
	8.31	1.59	2.61	Shale	
	20.73	2.44	5.05	Shale	
	12.98	51.24	56.29	Fractured shale	
	5.89			Fractured shale	
23	99.38			Shale	H
24	242.1	1.46	1.46	Top soil	HQ
	67.47	1.25	2.7	Shale	
	0.66	0.24	2.95	clay	
	93.55	14.12	17.06	shale	
	9.27			Fractured shale	
25	328.53	1.01	1.01	Top soil	K
	123.1	4.47	5.48	Shale	
	3.86	1.34	6.81	Clay	
	16554	143.32	150.14	Sandstone	
	10.25			Fractured shale	

Table 2 (continued)

VES No	Resistivity (Ωm)	Thickness (m)	Depth (m)	Inferred Lithology	Curve Type
26	1053.8	2.69	2.69	Top soil	HQ
	212.07	10.5	13.2	Shale	
	139.72	44.37	57.57	Shale	
	7926.3			Sandstone	
27	151.28			Shale	Q
28	177.91			Shale	HK
29	201.29	0.41	0.41	Top soil	HK
	1630.7	1.42	1.83	Sandstone	
	75.37			Shale	
30	304.19	3.57	3.57	Top soil	H
	18.84	8.25	11.82	Fractured shale	
	80.99			Shale	
31	191.08	2.1	2.1	Top soil	HK
	4.63	3.17	5.27	Clay	
	39.41			Fractured shale	
32	491.56	1.12	1.12	Top soil	Q
	184.56	5.22	6.34	Shale	
	2.15	0.51	6.85	clay	
	112.11	22.25	29.1	Shale	
	1.11			Fractured shale	
33	303.19	1.38	1.38	Top soil	Q
	75.3	0.67	1.39	Shale	
	85.61	2.92	4.31	Shale	
	146.71	13.33	17.64	Shale	
	16.95			Fractured shale	
34	125.59	2.31	2.31	Top soil	HK
	161.89	6.37	8.68	shale	
	11.76			Fractured shale	
35	535.53	1.2	1.2	Top soil	HK
	608.83	0.62	1.82	Sandstone	
	107.33			Fractured sandstone	
36	193.77	1.67	1.67	Top soil	H
	20	4.21	5.88	shale	
	34.45	38.14	44.02	Fractured shale	
	1480.6			Sandstone	
37	3949.3	0.88	0.88	Top soil	HK
	83.48	3.55	4.43	Shale	
	3.55	1.86	6.29	Clay	
	36.82			Fractured shale	
38	445.32	0.32	0.32	Top soil	HK
	360.7	4.99	5.31	shale	
	48.18	36.66	41.97	Fractured Shale	
	6039.6			Sandstone	
39	51.26			Fractured shale	H
40	1333.3	0.47	0.47	Top soil	H
	27.21	24.55	25.02	Fractured shale	
	2515.2			Sandstone	

a Plot of VES 2 at Azuiyiokwu, Abakaliki   **b** Plot of VES 7 at Mebiowa, Okposi   **c** Plot of VES 22 at Amike – Aba, Abakaliki

Fig. 3 Sample of VES plots in the study area. **a** Plot of VES 2 at Azuiyiokwu, Abakaliki, **b** Plot of VES 7 at Mebiowa, Okposi, **c** Plot of VES 22 at Amike – Aba, Abakaliki

Table 3 Sample of geoelectric sections

(a) Geoelectric section of VES 2				
Layer	Resistivity (Ωm)	Thickness (m)	Depth (m)	Geoelectric Section
1.	91.12	0.24	0.24	Top Soil
2.	131.97	0.21	0.45	Shale
3.	309.74	7.62	8.07	Shale
4.	40.32			Fractured shale
(b) Geoelectric section of VES 7				
Layer	Resistivity (Ωm)	Thickness (m)	Depth (m)	Geoelectric Section
1.	148.67	0.51	0.51	Top Soil
2.	119.64	4.17	4.68	Shale
3.	18.12	26.69	31.37	Fractured shale
4	7.38			Fractured shale
(c) Geoelectric section of VES 22				
Layer	Resistivity (Ωm)	Thickness (m)	Depth (m)	Geoelectric Section
1.	78.14	1.01	1.01	Top Soil
2.	8.31	1.59	2.61	Clay
3.	20.73	2.44	5.05	Shale
4.	12.98	51.24	56.29	Fractured shale
5.	5.89			Fractured Shale

electrodes C and D is as given in Eq. (3), while the resistivity is calculated using Eq. (4). For the Schlumberger array which was applied in this work, If $r_{AC} = r_{DB} = (L - a)/2$ and $r_{AD} = r_{CB} = (L + a)/2$, and substituting into the general formula, Eq. (4) turns to Eq. (5), which was applied in calculating the apparent resistivity of layers in this study:

$$V = \frac{\rho I}{2\pi} \left[\left(\frac{1}{r_{AC}} - \frac{1}{r_{CB}} \right) - \left(\frac{1}{r_{AD}} - \frac{1}{r_{DB}} \right) \right] \tag{3}$$

$$\rho = 2\pi \frac{V}{I} \left[\left(\frac{1}{r_{AC}} - \frac{1}{r_{CB}} \right) - \left(\frac{1}{r_{AD}} - \frac{1}{r_{DB}} \right) \right]^{-1} \tag{4}$$

$$U_C = \frac{\rho I}{2\pi} \left(\frac{1}{r_{AC}} - \frac{1}{r_{CB}} \right) \tag{1}$$

$$\rho = 2\pi \frac{V}{I} \left[\left(\frac{2}{L - a} - \frac{2}{L + a} \right) - \left(\frac{2}{L + a} - \frac{2}{L - a} \right) \right]^{-1}$$

$$U_D = \frac{\rho I}{2\pi} \left(\frac{1}{r_{AD}} - \frac{1}{r_{DCB}} \right) \tag{2}$$

$$\Rightarrow \rho = \frac{\pi V}{4I} \left(\frac{L^2 - a^2}{a} \right) \tag{5}$$
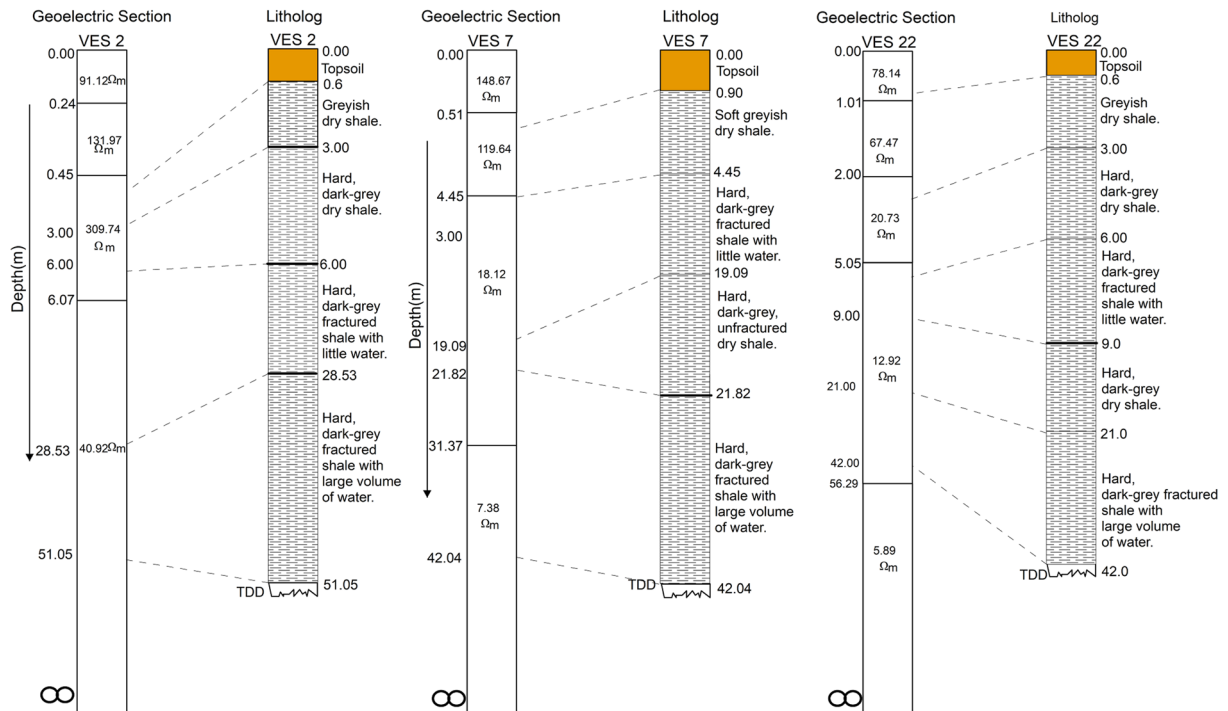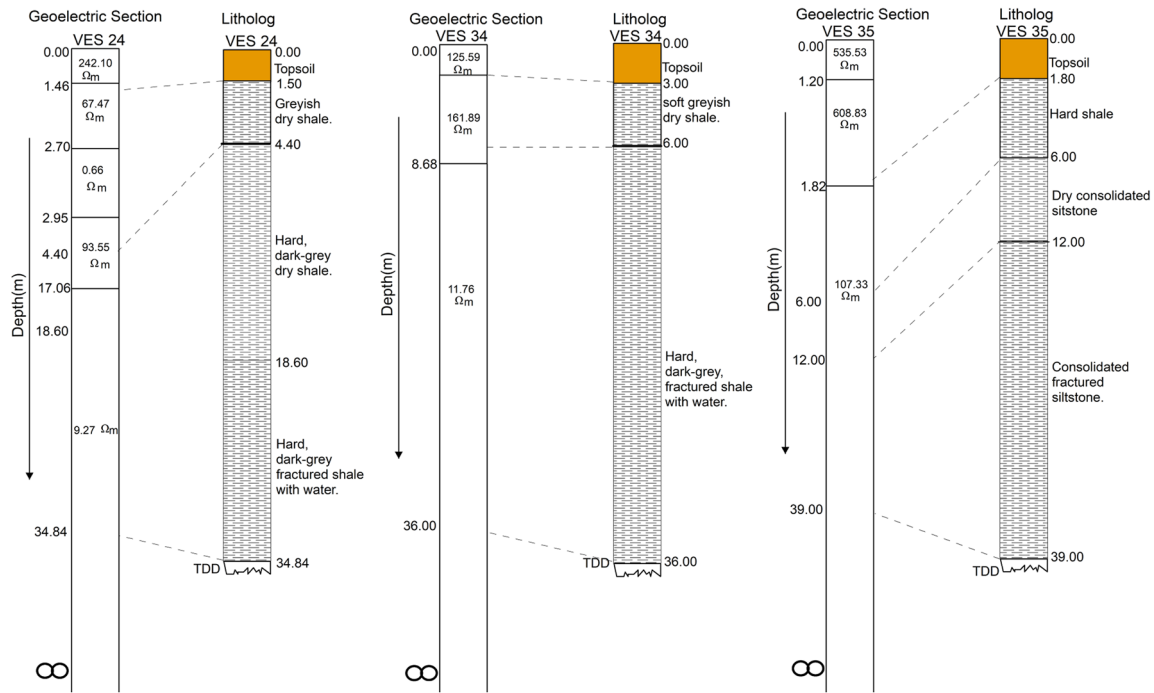
Fig. 4 **a** Correlation of Borehole logs with their geoelectric sections at VES 2, 7, and 22. **b** Correlation of Borehole logs with their geoelectric sections at VES 24, 34, and 35

Since the area is associated with shallow aquifers, the depth of investigation was good enough for this research. At each VES point, traverse directions were measured with a compass and coordinates were taken with GPS. The resulting resistance of each VES point was recorded in a survey datasheet. The calculated apparent resistivities were plotted against the electrode spacing (AB/2) to generate the relevant geoelectric curves. The processing of the data was enhanced with the use of interpex IX1D software, which enabled the generation of geoelectric layers.

Six exploration wells were randomly sited for this study. The primary target of these wells was the Asu River Group shales and sandstone. By applying the Logging While Drilling (LWD) approach, lithologic logs (Lithologs) were produced from these exploration wells using rock cuttings from the wells. A correlation of the lithologs with their geoelectric sections enhanced the delineation of zones of groundwater occurrence in relation to their resistivity ranges. To infer lithologies associated with the different geoelectric sections, field observation of the top soil at the point of survey, coupled with the knowledge gotten from the results of the correlations carried out in the present work, was integrated with the works of Telford et al. (1990) and Keary et al. (2002). Finally, the spatial distribution of resistivity at the subsurface was modeled using arc–GIS software.

Result and discussion

Results of the VES survey in the area are as represented in Table 2. From Table 2, it can be observed that some of the geoelectric layers inferred as shales have relatively high resistivity values which are quite comparable with that of sandstones. This is as a result of baking of the shales due to tectonism and magmatism in the area (Benklelil 1989). This diagenetic alteration increased the density of the shales in the area, especially those of Asu River Group, above those of the volcanic rocks intruding the shales and very close to its sandstone members (Obasi and Selemo 2018); even

the volcanic rocks in the study area displayed higher porosity than the shales, while those of the sandstones are quite correlatable with the porosity of the shales. The shales are so indurated that they are used as construction materials (Okogbue and Nweke 2018; Obasi et al. 2020). Sandstones/siltstones occurrence in the study area is in lenses (Agumanu 1989), while the majority of the rock units are shales and mudstones. Hence, except for the places where there are indications of sandstone occurrence and/or very high resistivity values, most of the surveys were carried out in shale-dominated environments. Consequently, based on the level of induration of the shales, it is not strange to associate them with some relatively high resistivity values when they are in a fresh and unfractured state.

Representative samples of the bi-log plots of apparent resistivity against $^{AB}/_2$ in the study area and their corresponding geoelectric sections are as shown in Fig. 3 and Table 3, respectively. Exploration wells were drilled at the locations of Fig. 3a–c, respectively. They all cut through fractured zones and supplied water at economic quantity. VES 2 has K curve type, while VES 7 and 22 have Q curve type. Three more exploration wells were drilled at VES locations 24, 34, and 35. Their curve types are HQ (VES 24), and HK (VES 34 and 35). All the six wells are productive at economic quantity. This suggests that there is no specific resistivity curve type that is uniquely associated with groundwater-bearing fractures in the study area. The geoelectric section of VES 2 (Table 3a) indicates that the resistivity of the shales can be above 300 Ωm, and increases with the depth of burial (see layers 2–4 on Table 3a), except for the fractured zones. Within the fresh and unfractured zones, the shallower the depth of occurrence of the shales, the less indurated they are, and the lower its resistivity (see Table 3a–c). Within the study area, soft, less-compacted, fresh, unfractured shales maintain the usual resistivity range of values as given by Telford et al. (1990), which are aquitards and are not expected to supply water at economic quantity. That could explain why the shales layers in VES 2, 5, 6, 7, 11, 12, 13, 14, 15, 16, 17, 22, 31, and 36 have resistivity

Table 4 Resistivity values for fractured rocks from different parts of the world

| S/No	Location	Rock type	Age	Saturated fracture zone resistivity Ωm	References
1	Eastern desert, Egypt	Shale	Eocene	≤ 22	Ammar and Kamal (2018)
2.	Eastern desert, Egypt	Limestone	Eocene	≤ 50	Ammar and Kamal (2018)
3.	Karnataka, India	Gneisses/Schist	Archaean	100 – 3000	Chandra et al. (2019)
4.	Abi, Nigeria	Shale	Albian	≤ 45	Ebong et al. (2014)
5.	Abi, Nigeria	Sandstone	Albian	100–800	Ebong et al. (2014)
6.	Bulawayo, Zimbabwe	Basalt	Archaean	< 50	Muchingami et al. (2012)
7.	Abakaliki, Nigeria	Shale	Albian	≤ 52	Present work
8.	Abakaliki, Nigeria	Sandstone	Albian	> 100	Present work
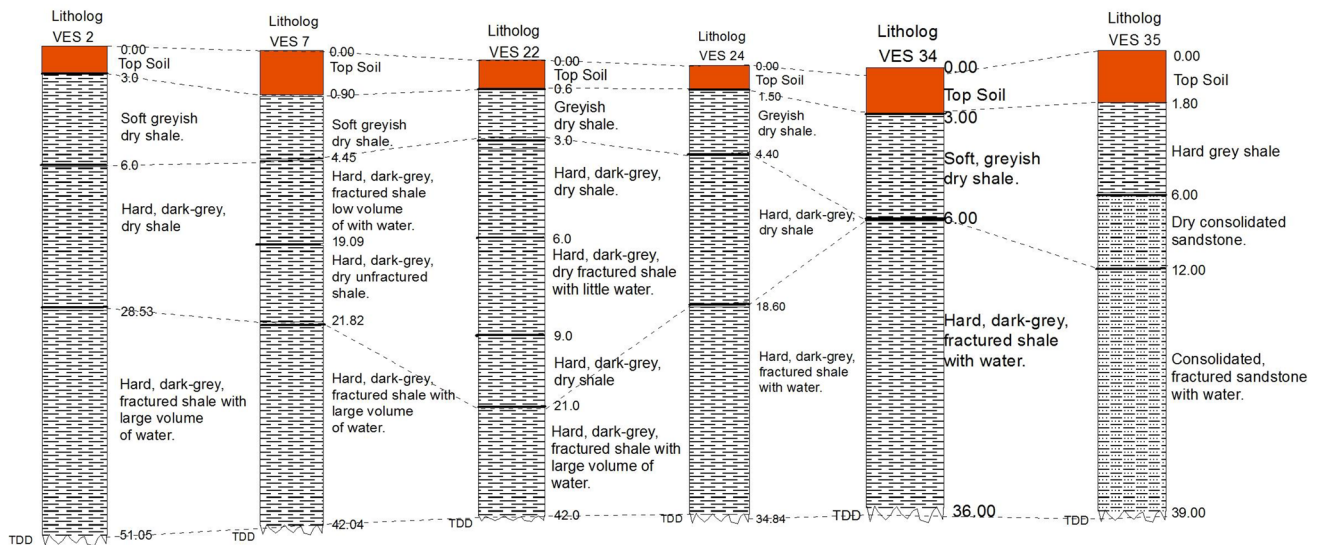
**Fig. 5** Well-to-well correlation of the six boreholes drilled in the study area

values which are ≤ 50.00 Ωm but not all were defined as fractured shales (see Table 2). All the soft and unfractured shales whose resistivities are ≤ 50.00 Ωm occurred at depth ranges of ≤ 10 m, which is not commonly associated with groundwater occurrence in the area. For the fractured shales which host groundwater, all their depth ranges are > 10 m.

A correlation of borehole logs from successful boreholes in the study area with the geoelectric layers of their corresponding VES data (Fig. 4) gave a near-perfect match of the surface geophysics with subsurface geology. The groundwater-bearing unit has a resistivity of 40.32 Ωm at VES 2, ≤ 18.12 Ωm at VES 7, ≤ 12.92 Ωm at VES 22, 9.27 Ωm at VES 24, 11.76 Ωm at VES 34, and 107.33 Ωm at VES 35. From Table 2, further resistivity values of water-bearing fractured zones include 29.85 Ωm, 23.39 Ωm, 12.07 Ωm, 50.15 Ωm, 24.63 Ωm, 32.73 Ωm, 36.50 Ωm, 14.46 Ωm, 4.38 Ωm, 1.76 Ωm, 4.27 Ωm, 10.25 Ωm, 39.41 Ωm, 1.11 Ωm, 16.95 Ωm, 34.45 Ωm, 36.82 Ωm, 48.18 Ωm, 51.26 Ωm, and 27.21 Ωm which are for VES points 5, 6, 10, 11, 12, 13, 14, 15, 16, 20, 25, 31, 32, 33, 36, 37, 38, 39, and 40 respectively. VES 35 is the only exploration borehole dug into a fractured sandstone unit. The other five boreholes were dug through a fractured shale unit. The above result suggests that geoelectric layers within the shale lithology with a resistivity range of ≤ 52 Ωm at depth represent water-bearing fracture zones. Low-resistivity anomalies are generally associated with flow features such as faults and fractures with fluids and higher porosity lithologies (Ammar and Kamal 2018; Houston and Lewis 1988). Correlated data at VES 2 and 22 (Fig. 4) indicate that the lower the resistivity at fracture zone in the shales at depth (i.e., as $\rho \to 0$), the wider the fracture, which increases the volume of water available to the well bore. The shales in the study area are rich in clay

minerals such as illite, chlorite, and kaolinite. An increase in depth of burial leads to the increase in chlorite and illite occurrence due to the diagenetic conversion of kaolinite to chlorite and illite (Agumanu 1989). Chlorite often contains iron and magnesium in its structure, which can enhance the current flow. A high concentration of iron oxide (Fe_2O_3) in the shales in this study has been earlier reported (Obiora and Charan 2011). As chlorite increases with the depth of burial, more oxides of iron and magnesium are available. During tectonism, the tectonic forces which created the faults/fractures pulverized some of the rocks along the fault/fracture planes and deposited them in situ. As water occupies these fractures, the Fe^{2+} and Mg^{2+} ions become mobile and conductive, thereby increasing conductivity within the fracture zone. With an increase in the wideness of fractures, both vertically and horizontally, a higher volume of water is stored within these fractures. Consequently, more ions are available to participate in the conductivity of currents, and the resistivity becomes further reduced. The impact of a high concentration of ions from clay minerals in reducing the resistivity of water-bearing fractured rocks has also been discussed by Armada et al. (2009). The resistivity character of the fractured shale zone in the study area is similar to that of clay in a less tectonically disturbed sedimentary basin (Kearey et al. 2002). The above result is quite correlatable to values from fractured sediments from other parts of the world (Table 4). A correlation of borehole log at VES 35 with its geoelectric section (Fig. 4) indicates that resistivity values for groundwater-bearing fractured sandstone in the study area are much higher than that of their shale counterparts. However, its value is much lower than the resistivity range for aquiferous sandstone units in the post-Santonian basins such as the Anambra and Niger Delta
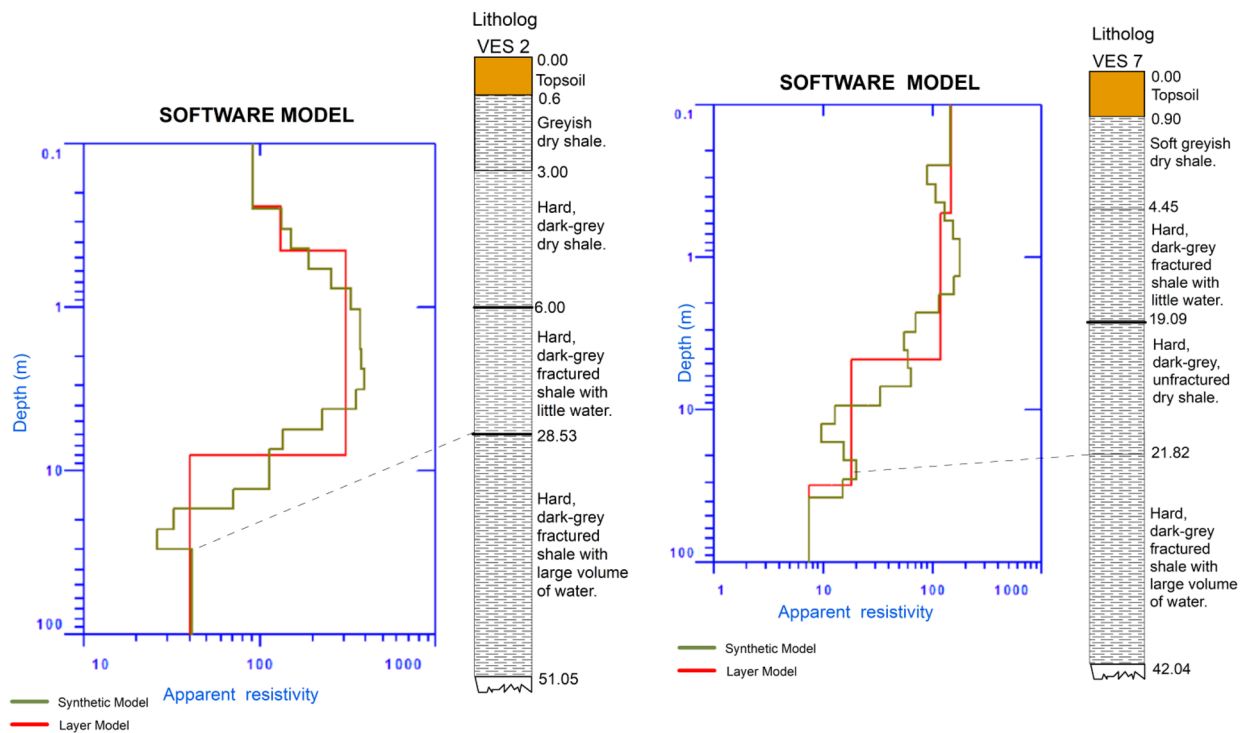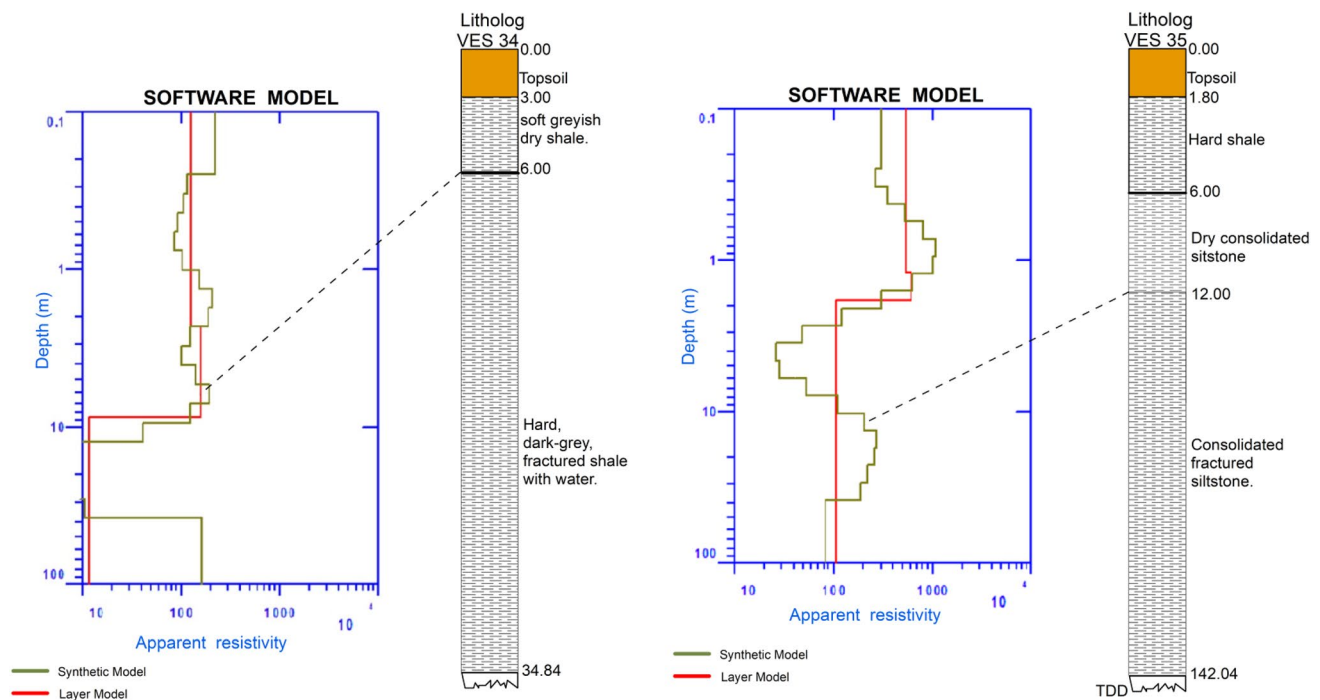
a Correlation of borehole logs with software models at VES 2 and 7.
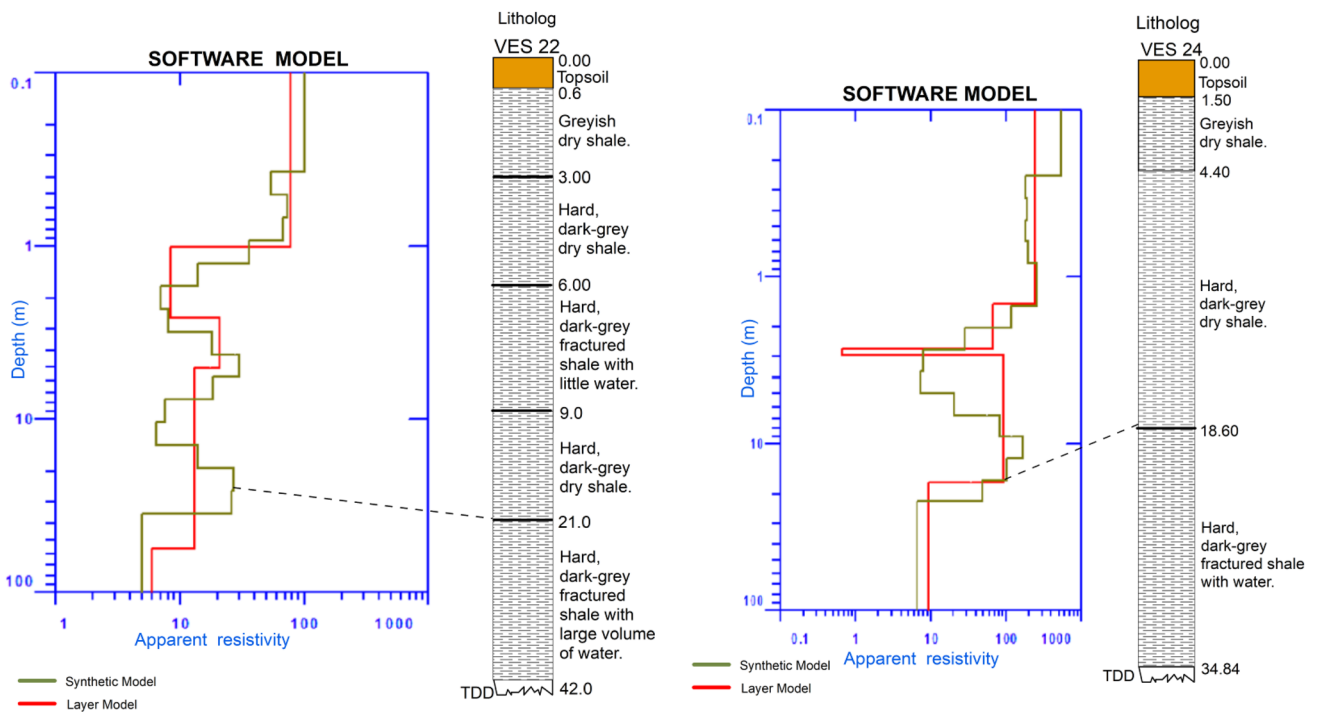
b Correlation of borehole logs with software models at VES 22 and 24

Fig. 6 Correlation of borehole logs with software models. **a** Correlation of borehole logs with software models at VES 2 and 7. **b** Correlation of borehole logs with software models at VES 22 and 24. **c** Correlation of borehole logs with software models at VES 34 and 35

c Correlation of borehole logs with software models at VES 34 and 35

Fig. 6 (continued)

Basins in southern Nigeria (Selemo et al. 1995), which have experienced less tectonic and digenetic alterations than the former. The result is also lower than the conventional resistivity range for sandstone aquifers (Telford et al. 1990).

The well-to-well correlation of the six exploration boreholes (Fig. 5) indicates that major water-bearing fractures occurred at depths ≥ 18 m in fractured shales and shallower in the fractured sandstones. However, at < 18 m depth, some minor fractures exist which could not supply water at economic quantity. Hence, groundwater exploration in the shales must target a depth range of ≥ 18 m.

A geoelectric layer with a mean resistivity in the range of ≤ 52 Ωm does not imply a 100% fractured shale unit. It was observed that while the layer model gives insight to the geoelectric layer with groundwater at economic quantity using its mean resistivity values, the synthetic model defines the depth to the top of the groundwater occurrence within the layer (Fig. 6). It can be observed from Fig. 6 that as the geoelectric section approaches the water-bearing fracture zone, both the layer and the synthetic models begin to have a near-perfect match. Any point of wide separation between the two models could be seen as the end of the fracture.

Hence, from the correlation of the borehole lithologs and layer models (Fig. 6), it was observed that the exploration wells at VES 2, 7, 22, 24, and 35 did not penetrate the total thickness of the fractured zone. Conversely, at VES 34, the total thickness of the fractured aquifer was penetrated by the well bore. The base of the fracture was marked in the layer model by the wide separation of the two models, with the synthetic model having very high resistivity value compared with its layer model counterpart. Suffice it to say that the synthetic model signature has been found useful, in this study, in mapping the total thickness of the fracture zone (Fig. 7) in the study area.

An evaluation of the spatial distribution of resistivity at the subsurface indicates that there is a resultant increase in resistivity with an increase in depth in the study area (Fig. 8). This could be related to the age and burial history of the rocks (Obasi and Selemo 2018) which has highly altered their physical and chemical properties. The spatial maps (Fig. 8) show that the water-bearing fractures extend from a depth of about 10 m to even beyond 80 m depth. They start as minor fractures at 10 m depth, became wider and more pronounced at 20–30 m depth, and then approximately

Fig. 7 Total thickness of the water-bearing fracture zone mapped with synthetic model signature

---- Synthetic Model

---- Layer Model
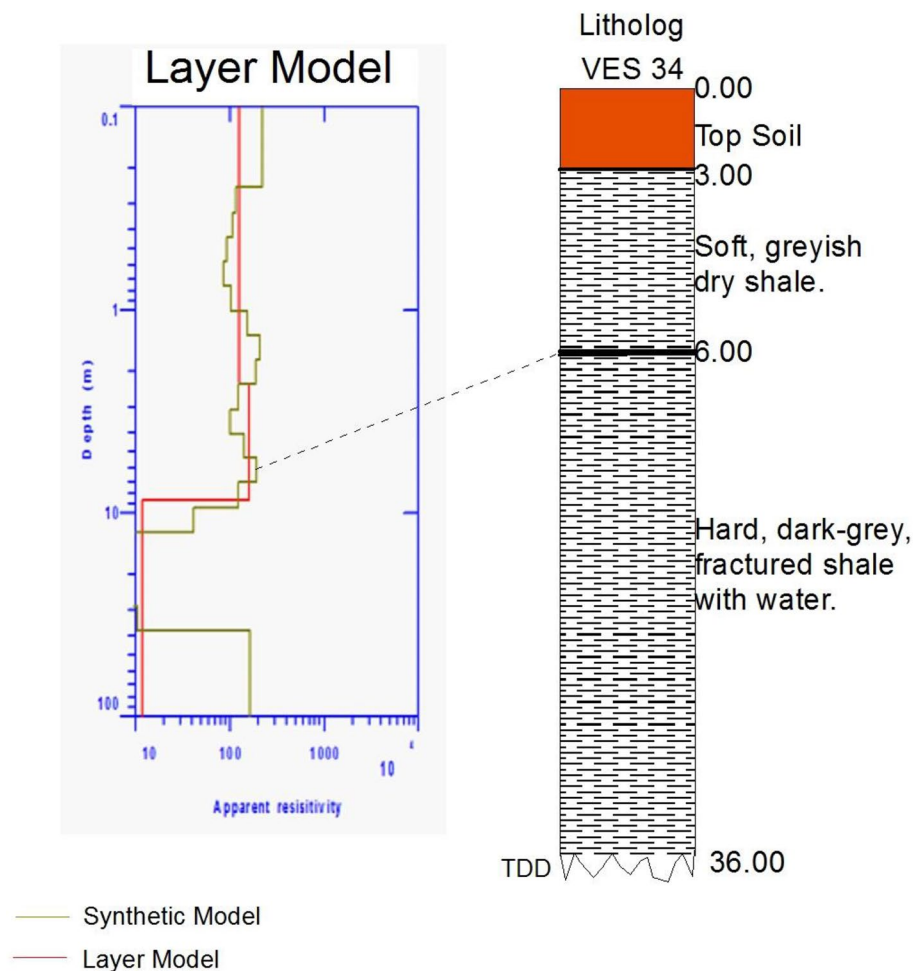
maintained a uniform thickness up to 80 m depth. At greater depths, the observed fractures continued narrowing to complete disappearance at about 100 m depth. This could explain why most drilled boreholes in the area are < 100 m deep. Field observations showed that groundwater in the study area has occurred at an economic quantity at a depth range of 20–80 m. Below 80 m, the water volume begins to drop gradually. Figure 8 also suggests the applicability of resistivity models in subsurface mapping. Migration from shale-dominated horizon to deeper sandstone zones can be observed (see Figs. 1 and 8a–f). However, some local variations occurred due to minor changes in the physical properties of the rocks such as the presence of fracture zones with groundwater.

Conclusion

An integration of bulk resistivity of the subsurface lithology generated from a 1-D resistivity survey with borehole lithologs has enabled the delineation of resistivity range for groundwater-bearing fracture zone in the fractured shales and sandstones in Abakaliki area, southern Benue Trough, Nigeria. The high correlatability between the geoelectric sections and lithologs has proved the efficacy of vertical electrical sounding in delineating the water-bearing fracture zones in the region. The vertical and lateral extents of the identified fractures have been well modeled using the spatial distribution map of resistivity of the area, while areas susceptible to borehole failure have been delineated. The application of the models from the present work in groundwater exploration in fractured sediments will reduce the rate of borehole failure in the area.
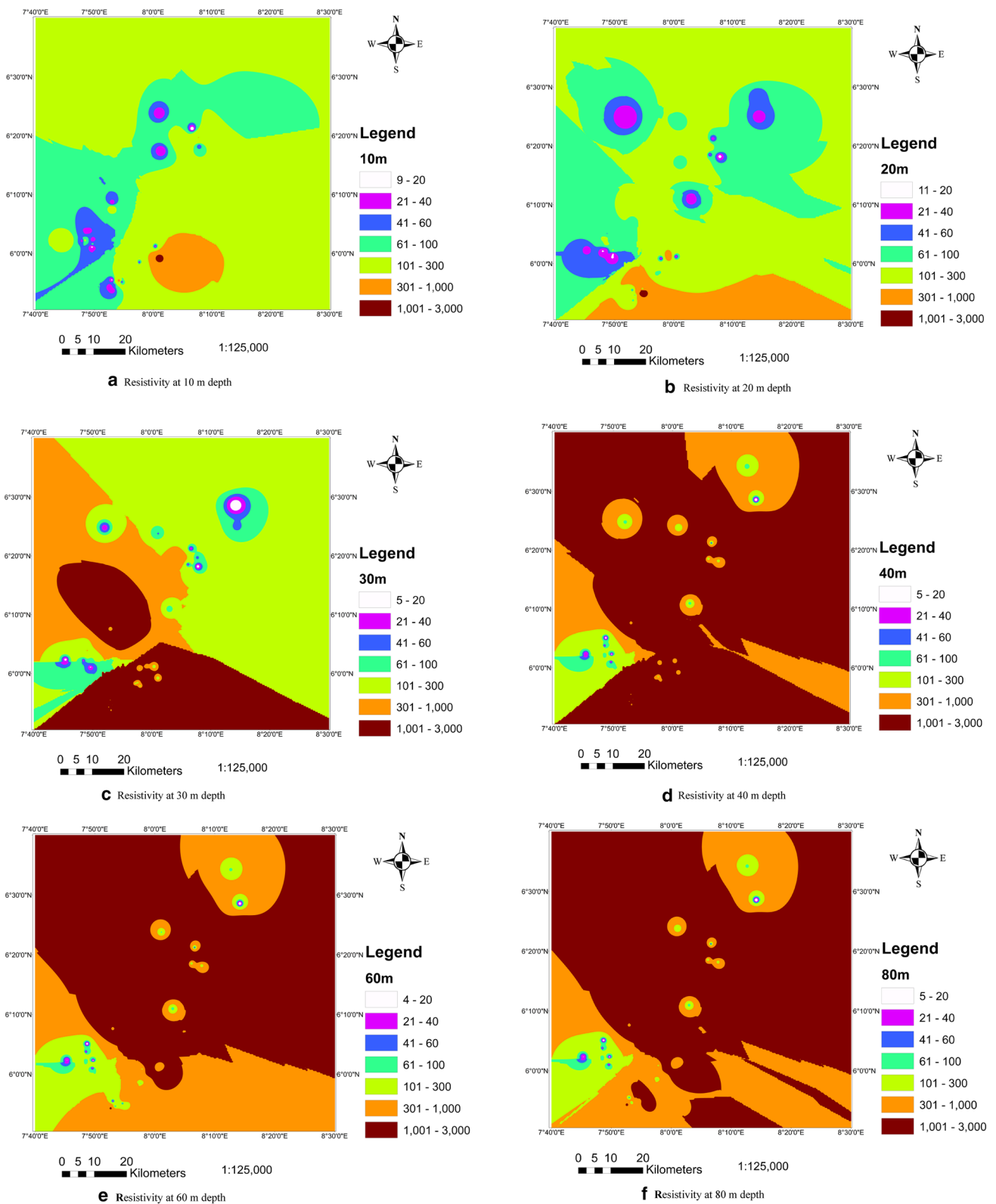
Fig. 8 Spatial distribution of resistivity at depths in the study area. **a** Resistivity at 10 m depth, **b** Resistivity at 20 m depth, **c** Resistivity at 30 m depth, **d** Resistivity at 40 m depth, **e** Resistivity at 60 m depth, **f** Resistivity at 80 m depth

Compliance with ethical standards

Conflict of interest   The authors declare that they have no conflict of interest.

References

Adepelumi AA, Yi MJ, Kim JH, Ako BD, Son JS (2006) Integration of surface geophysical methods for fracture detection in crystalline bedrocks of southwestern Nigeria. Hydrogeol J 14:1284–1306. https://doi.org/10.1007/s10040-006-0051-2

Agha SO (2015) Groundwater studies in abakaliki using electrical resistivity method. IOSR J Appl Phys 7(6):05–10

Aghamelu OP, Ezeh HN, Obasi AI (2013) Groundwater exploitation in the Abakaliki metropolis (southeastern Nigeria): issues and challenges. Afr J Environ Sci Technol 7(11):1018–1027

Agumanu AE (1989) The Abakaliki and Ebonyi formations: subdivisions of the Albian Asu River Group in the southern Benue Trough, Nigeria. J Afr Earth Sci 9:195–207

Akhter G, Hasan M (2016) Determination of aquifer parameters using geoelectrical sounding and pumping test data in Khanewal District, Pakistan. Open Geosci 8(1):630–638

Akpan AE, Ugbaja AN, George NJ (2013) Integrated geophysical, geochemical and hydrogeological investigation of shallow groundwater resources in parts of the Ikom-Mamfe Embayment and the adjoining areas in Cross River State, Nigeria. J Environ Earth Sci 70:1435–1456

Ammar AI, Kamal KA (2018) Resistivity method contribution in determining of fault zone and hydro-geophysical characteristics of carbonate aquifer, Eastern Desert, Egypt. Appl Water Sci 8:1. https://doi.org/10.1007/s13201-017-0639-9

Anosike JC, Nwoke BEB, Dozie I, Thofern UAR, Okere AN, Tony RN, Nwosu DC, Oguwuike UT, Dike MC, Alozie JI, Okugun GAR, Ajero CMU, Onyirioha CU, Ezike MN, Ogbusu FI, Ajayi EG (2003) Control of endemic dracunculiasis in Ebonyi state, Southeastern Nigeria. Int J Hyg Environ Health 206:591–596

Arabi SA, Dewu BBM, Muhammad AM, Ibrahim MB, Abafoni JD (2008) Determination of weathered and fractured zones in part of the basement complex of North-Eastern Nigeria. J Eng Technol Res 2(11):213–218

Armada LT, Dimalanta CB, Yumul GP, Tamayo RA (2009) Georesistivity signature of crystalline rocks in the Romblon Island Group, Philippines. Philippine J Sci 138(2):191–204

Barker RD, White CC, and Houston JFT (1992) Borehole sitting in an African accelerated drought relief project In: Wright EP, Burgess WGE (eds) Hydrogeology of crystalline basement aquifers in Africa. Geological Society London Special Publications 66(1): 183–201

Benkhelil J (1987) Structural frame and deformations in the Benue Trough of Nigeria. Bull Centres Rech Explor-Prod Elf- Aquitaine 11:160–161

Benkhelil J (1989) The origin and evolution of the Cretaceous Benue Trough, Nigeria. J Afr Earth Sci 8:251–282

Berryman JG, Hoversten GM (2013) Modelling electrical conductivity for earth media with macroscopic fluid-filled fractures. Geophys Prospect 61:471–493

Carbonel D, Gutiérrez F, Linares R et al (2013) Differentiating between gravitational and tectonic faults by means of geomorphological mapping, trenching and geophysical surveys. The case of the Zenzano Fault (Iberian Chain, N Spain). Geomorphology 189(1):93–108

Carruthers RM, and Smith IF, 1992. The use of ground electrical survey methods for siting water-supply boreholes in shallow crystalline basement terrains. In: Wright EP, Burgess WGE (eds) Hydrogeology of crystalline basement aquifers in Africa. Geological Society London Special Publications 66(1): 203–220

Chandra S, Auken E, Maurya PK, Ahmed S, Verma SK (2019) Large scale mapping of fractures and groundwater pathways in crystalline Hardrock By AEM. Sci Rep 9:398. https://doi.org/10.1038/s41598-018-36153-1

Chukwu A, Obiora SC (2018) Geochemical constraints on the petrogenesis of the pyroclastic rocks in Abakaliki basin (Lower Benue Rift), Southeastern Nigeria. J Afr Earth Sci 141:207–220

Comte JC, Cassidy R, Nitsche J, Ofterdinger U, Pilatova K, Flynn R (2012) The typology of Irish Hard-Rock Aquifers based on an Integrated Hydrogeological and Geophysical Approach. Hydrogeol J 20:1569–1588. https://doi.org/10.1007/s10040-012-0884-9

Demirel S, Roubinet D, Irving J, Voytek E (2018) Characterizing near-surface fractured-rock aquifers: insights provided by the numerical analysis of electrical resistivity experiments. Water 10:1117. https://doi.org/10.3390/w10091117

Ebong DE, Akpan AE, Onwuegbuche AA (2014) Estimation of geohydraulic parameters from fractured shales and sandstone aquifers of Abi (Nigeria) using electrical resistivity and hydrogeologic measurements. J Afr Earth Sci 96:99–109

El-Hussaini AH, Ibrahim HA, Bakhelt AA (1995) Interpretation of geoelectrical data from an area of the entrance of Wadi Qena, eastern Desert, Egypt. J King Saudi Univ 7:257–276

Famiglietti JS (2014) The global groundwater crisis. Nat Clim Change 4(11):945–948

Freeze RA, Cherry JA (1979) Groundwater. Prentice-Hall Inc, Englewood Chiffs

Gao Q, Shang Y, Hasan M et al (2018) Evaluation of a weathered rock aquifer using ERT Method in South Guangdong, China. Water 10(3):293

Genik GJ (1993) Petroleum geology of Cretaceous—Tertiary basins in Niger, Chad and Central African Republic. Assoc Petrol Geol Bull 77:1405–1434

Griffiths DH, Barker RD (1993) Two-dimensional resistivity imaging and modeling in areas of complex geology. J Appl Geophys 29(3):211–226

Hasan M, Shang Y, Jin W (2018a) Delineation of weathered/fracture zones for aquifer potential using an integrated geophysical approach: a case study from South China. J Appl Geophys 157:47–60

Hasan M, Shang Y, Akhter G et al (2018b) Evaluation of groundwater potential in Kabirwala area, Pakistan: a case study by using geophysical, geochemical and pump data. Geophys Prospect 66(9):1737–1750

Hasan M, Shang Y, Jin W, Akhter G (2019) Investigation of fractured rock aquifer in South China using electrical resistivity tomography and self-potential methods. J Mt Sci 16(4):850–869

Houston JFT, Lewis RT (1988) The Victoria province drought relief project. II. Borehole yield relationships. Groundwater 26:418–426

Improta L, Ferranti L, De Martini PM et al (2010) Detecting young, slow-slipping active faults by geologic and multidisciplinary high-resolution geophysical investigations: a case study from the Apennine seismic belt, Italy. J Geophys Res 115(B11307):1–26

Jinsong S, Benyu S, Naichuan G (2009) Anisotropic characteristics of electrical responses of fractured reservoir with multiple sets of fractures. Pet Sci 6:127–138

Krasny J (2002) Quantitative hardrock hydrogeology in a regional scale. Norges Geologiske Undersøkelse Bulletin 439:7–14

Loke MH, Acworth I, Dahlin T (2003) A comparison of smooth and blocky inversion methods in 2D electrical imaging surveys. Explor Geophys 34(1):182–187

Lucas DR, Fankhauser K, Springman SM (2016) Application of geotechnical and geophysical field measurements in an active alpine environment. Eng Geol 219:32–51

MacDonald AM, and Davies J, 1998. The Hydrogeology of the Oju, Obi Area, Eastern Nigeria: Adega, Ojokwe (Southern Oju), Ohuije, Ijokwe (Obi) and Akiraba-Ainu data report. British Geological Survey Technical Report Wc/98/70r

MacDonald AM, Bonsor HC, Dochartaigh B, Taylor RG (2012) Quantitative maps of groundwater resources in Africa. Environ Res Lett 7:024009. https://doi.org/10.1088/1748-9326/7/2/024009

Murat RC, 1970. Stratigraphy and Palaeogeography of Cretaceous and Lower Tertiary in Southern Nigeria. 1st Conference on African Geology, Ibadan Proceedings. Ibadan University Press

Nnamani MN, Nnabueze UC (2012) Evaluation of guinea worm eradication programme in Ebonyi State, Nigeria. Acad Res Int 3(2):451–460

Nwajide CS (2013) Geology of Nigeria's sedimentary basins. CSS Bookshop Limited, Lagos

Nwajide CS, and Reijers TJ, 1996. The geology of the southern Anambra Basin. In: TAJ Reijers (Eds), Selected Chapters on Geology: Sedimentary Geology and Sequence Stratigraphy of the Anambra Basin. SPDC publ, pp. 133–148

Obasi AI, Selemo AOI (2018) Density and reservoir properties of Cretaceous rocks in southern Benue Trough, Nigeria: implications for hydrocarbon exploration. Arab J Geosci 11:307. https://doi.org/10.1007/s12517-018-3634-z

Obasi AI, Ogwah C, Selemo AOI, Afiukwa JN, Chukwu CG (2020) In situ measurement of radionuclide concentrations (238U, 40 K, 232Th) in middle Cretaceous rocks in Abakaliki-Ishiagu areas, southeastern Nigeria. Arab J Geosci 13:374. https://doi.org/10.1007/s12517-020-05360-4

Obiora SC, Charan SN (2011) Geochemistry of regionally metamorphosed sedimentary rocks from the lower Benue Rift: implications for provenance and tectonic setting of the Benue Rift. S Afr J Geol 114(1):25–40

Obiora SC, Umeji AC (2004) Petrographic evidence for regional burialmetamorphism of the sedimentary rocks in the lower Benue rift. J Afr Earth Sci 38:269–277

Odoh BI, Utom AU, Nwaze SO (2012) Groundwater prospecting in fractured shale aquifer using an integrated suite of geophysical methods: a case History From Presbyterian Church, Kpiri-Kpiri, Ebonyi State, SE Nigeria. Geosciences 2(4):60–65

Okeke PO, Sowa A, Selemo AO, Iheagwu MC (1987) The thickness of the Cretaceous sediments in the southern Benue Trough, Nigeria, its tectonic implications. In: Matheis Schandelmeier (ed) Current research in African earth sciences. Balkema, Rotterdam, pp 295–298

Okogbue C, Nweke M (2018) The 226Ra, 232Th and 40 K contents in the Abakaliki baked shale construction materials and their potential radiological risk to public health, southeastern Nigeria. J Environ Geol 2(1):13–19

Olorunfemi MO, Oni AG (2019) Integrated geophysical methods and techniques for siting productive boreholes in basement complex terrain of southwestern Nigeria. Ife J Sci 21(1):13–26

Onwe IM, Otosigbo GO, Eluwa NN, Nkitnam EE (2019) Geoelectrical and hydrochemical assessment of groundwater for potability in Ebonyi North, Southeastern Nigeria. Int J Geol Min 5(1):237–244

Petters SW (1980) Biostratigraphy of upper Cretaceous foraminifera of the Benue Trough Nigeria. J Foraminifer Res 10:191–204

Selemo AOI, Okeke PO, Nwankwo GI (1995) An appraisal of the usefulness of vertical electrical sounding (VES) in groundwater exploration in Nigeria. Water Resour 6(1 & 2):61–67

Steelman CM, Kennedy CS, Capes DC, Parker BL (2017) Electrical resistivity dynamics beneath a fractured sedimentary bedrock riverbed in response to temperature and groundwater–surface water exchange. Hydrol Earth Syst Sci 21:3105–3123

Taylor RW, Fleming AH (1988) Characterizing jointed systems by azimuthal resistivity surveys. Ground Water 26:464–474

Telford WM, Geldart LP, Sheriff RE, Keys DA (1990) Applied geophysics. Cambridge University Press, New York

Tizro AT, Voudouris KS, Salchzade M, Mashayekhi H (2010) Hydrogeological framework and estimation of aquifer hydraulic parameter using geoelectrical data: a case study from West Iran. Hydrogeol J 18:917–929

Ugwu SA, Nwosu J (2009) Detection of Fractures for Groundwater Development in Oha Ukwu using Electromagnetic Profiling. J Appl Sci Environ Manage 13(4):59–63

Vchery A, Hobbs B (2003) Resistivity imaging to determine clay cover and permeable units at an ex-industrial site. Near Surf Geophys 1:21–30

Wolfe E (2007) Dracunculiasis eradication global surveillance summary, 2006 weekly Epidemiological Record. 82:133-140